Carbazole isomer induces ultralong organic phosphorescence

Chengjian Chen[1], Zhenguo Chi[2], Kok Chan Chong[1], Andrei S. Batsanov[3], Zhan Yang[2], Zhu Mao[2], Zhiyong Yang[2], Bin Liu[1,4]*

[1]Department of Chemical and Biomolecular Engineering, National University of Singapore, 4 Engineering Drive 4, Singapore 117585, Singapore.

[2]School of Chemistry, Sun Yat-sen University, Guangzhou 510275, China.

[3]Department of Chemistry, Durham University, Durham DH1 3LE, UK.

[4] Joint School of National University of Singapore and Tianjin University, International Campus of Tianjin University, Binhai New City, Fuzhou 350207, China

*Corresponding author. Email: cheliub@nus.edu.sg

Commercial carbazole (Cz) has been widely used to synthesize organic functional materials that have led to recent breakthroughs in ultralong organic phosphorescence[1], thermally activated delayed fluorescence[2,3], organic luminescent radicals[4] and organic semiconductor lasers[5]. However, the impact of low concentration isomeric impurities present in commercial batches on the properties of the synthesized molecules requires further analysis. Here, we synthetized highly pure Cz (Lab-Cz), and observed that its fluorescence is blue-shifted by 54 nm with respect to commercial samples whereas its room-temperature ultralong phosphorescence almost disappears[6]. We discover that such differences are due to the presence of a Cz isomeric impurity in commercial Cz sources, with concentration <0.5 mol%. Ten representative Cz derivatives resynthesized from the Lab-Cz failed to show the ultralong phosphorescence reported in previous literature[1,7-15]. However, phosphorescence is recovered by adding 0.1 mol% isomers, which act as charge traps. Investigating the role of isomers can therefore provide alternative insight on the mechanisms behind ultralong organic phosphorescence[1,6-18].

Ultralong phosphorescence, also called afterglow, is resulted from the storage of excitation energy and slow release of luminescence mainly *via* triplet states[19,20]. The first scientifically documented afterglow material was Bologna Stone and its afterglow was caused by impurity doping[21]. Two decades ago, the research interest of inorganic afterglow was heated up by doping Dy^{3+} into the $SrAl_2O_4:Eu^{2+}$ phosphor[22]. Nowadays, inorganic afterglow has been extensively employed to produce luminous paints, dials, emergency signs and so on[19]. As compared to the inorganic counterpart, organic materials show more advantages, such as flexibility, transparency, solubility and color tunability[20]. Recently, organic afterglow materials including carbazole, dibenzothiophene, dibenzofuran, fluorene and their derivatives have been successfully developed[14]. However, their impurity hypotheses have been under debate since the early 20th century[6,15,23], but without solid evidence. For example, through sublimation and recrystallization, small traces of impurities were proposed to contribute to phosphorescence[23], while the impurity effect was ruled out by the explanation of crystal quality nearly 40 years later[6]. Notably, the phosphorescence of many solid organic compounds was attributed to very small traces of impurities[15,23]. Therefore, identifying the molecular structure of impurity conundrum is critical to build frameworks for efficient utilization of triplet states in organic functional materials.

More than a century ago, carbazole (Cz) was successfully isolated from the anthracene fraction of coal tar[24], which is the current commercial source of Cz. During the past 5 years, Cz derivatives have attracted much research interest, and many of them have directly led to the recent breakthroughs, such as highly efficient delayed fluorescence emitters[2,3], efficient organic luminescent radicals[4] and organic semiconductor lasers[5]. In particular, commercial Cz derivatives are the current focus of single-component organic ultralong phosphorescence studies[1,6-14,16-18]. However, fundamental inconsistencies emerged when the same compounds were repeatedly reported by different research groups[7-12,15]. We therefore examined the commercial Cz from Tokyo Chemical Industry (TCI), J&K, Sigma-Aldrich (Sigma) and Aladdin. All of them showed room-temperature ultralong phosphorescence after recrystallization[6], but with varied intensities and durations. Moreover, we also tried to purify Cz of TCI (TCI-Cz) using column chromatography three times with dichloromethane/hexane (1/3, v/v), ether acetate/hexane (5/95, v/v) and dichloromethane/hexane (1/2, v/v) as the eluents, respectively, which was followed by recrystallization from toluene. The obtained TCI-Cz still showed very bright room-temperature ultralong phosphorescence, clearly visible to naked eye.

We then synthesized Cz (Lab-Cz) from 2-aminobiphenyl (details in Methods). Surprisingly, the fluorescence of Lab-Cz is blue-shifted by 54 nm (Supplementary Fig. 1) and the well-known ultralong phosphorescence almost disappears as compared to that for TCI-Cz in the same crystal state (Fig. 1a)[6,8]. Notably, the room-temperature ultralong phosphorescence of Lab-Cz crystals could not be observed by naked eye. However, as shown in Supplementary Fig. 2, very weak luminescence from Lab-Cz could be captured by a Sony camera at 8.3 ms off 365 nm light illumination, and the signal disappeared after 83.3 ms. Under the same camera setting, the photos of TCI-Cz were all overexposed with strong luminescent and background signals. This result indicates that some small traces of impurities play a key role in ultralong phosphorescence.

To separate the impurities, many methods had been tried without success until high-performance liquid chromatography (HPLC) was rationalized to monitor the onset absorption at 346 nm. This wavelength was essential because when monitored at 294 nm (Fig. 1b), the signal of impurity was easily covered by the maximum absorption of the dominant Cz (Supplementary Fig. 3). However, at the onset absorption of 346 nm (Fig. 1c), the impurity peak is uncovered gradually when optimizing acetonitrile-water ratio from 95/5 to 50/50 (v/v). After isolating ~10 mg of the impurity from commercial TCI-Cz (details in Supplementary Methods), X-ray crystallography revealed its structure as an isomer of Cz, 1*H*-benzo[*f*]indole (Bd, Fig. 1c and Supplementary Fig. 4a). The isomer Bd itself does not show room-temperature ultralong phosphorescence even in the crystal state. We further identified the same impurity from Cz supplied by J&K, Sigma-Aldrich and Aladdin, but with different content (Figs. 1d, 2a and Supplementary Table 1). As the isomer Bd inherits similar reactivity to Cz, we speculate that this widespread isomer could affect a variety of organic materials derived from commercial Cz.

Taking CPhCz and DPhCzT (Figs. 2c, d) as the examples[1,7], the contribution of Bd to their reported ultralong phosphorescence was studied in detail. Considering Bd in commercial Cz (Fig. 2a), TCI-CPhCz (synthesized from TCI-Cz) was carefully purified by column three times before recrystallization (details in Supplementary Methods). In the same single crystal state (Fig. 2d), the purified TCI-CPhCz exclusively shows room-temperature ultralong phosphorescence in contrast to Lab-CPhCz (synthesized from Lab-Cz). Meanwhile, the optimized HPLC of the recrystallized TCI-CPhCz revealed a small trace of impurity upon monitoring at the onset absorption of 354 nm, which was later quantified to be 0.1 mol% (Fig. 2b). X-ray

crystallography identified its structure as CPhBd (Fig. 2c and Supplementary Fig. 4b), after isolating ~22 mg of the impurity from TCI-CPhCz. CPhBd itself does not show room-temperature ultralong phosphorescence in the crystal state. We further confirmed that CPhBd could be scaled up from Bd by using the same synthetic method as that of CPhCz from Cz (Supplementary Scheme 1)[7]. Similarly, following the procedure for DPhCzT from Cz[1], DPhBdT (Fig. 2c) was synthesized from Bd and no room-temperature ultralong phosphorescence was observed by naked eye.

To explore the generality of the phenomenon, another 8 representative Cz derivatives with reported ultralong phosphorescence were further tested (Supplementary Fig. 5)[1,7-15]. It was found that their reported ultralong phosphorescence was only observed by naked eye with the crystals synthesized from TCI-Cz, but not from Lab-Cz. Taken together, we propose that the isomer Bd in commercial Cz is responsible for their reported ultralong phosphorescence. This result also indicates that the widespread presence of Bd should be taken into consideration for other organic semiconductors directly synthesized from commercial Cz without proper exclusion of the isomer especially for those being used in optoelectronic applications[2-5,25]. The ultralong phosphorescence of Bd/Lab-Cz could be observed even at the presence of 0.01 mol% Bd (Supplementary Fig. 6b), implying that the isomer doping is extremely effective. This ultra-low content also explains why the impurity effect has been largely ignored so far[1,6-14].

To understand how the isomer affects ultralong phosphorescence, emission characteristics were investigated with 0 mol%, 0.5 mol%, 1 mol%, 5 mol%, 10 mol% and 100 mol% isomer dopants in crystalline states, respectively (Fig. 3 and Supplementary Fig. 7). The isomer doping effect of ultralong phosphorescence could be further corroborated since each pair of 0.5 mol% Bd/Lab-Cz and TCI-Cz (Fig. 3a), 0.5 mol% CPhBd/CPhCz and TCI-CPhCz (Fig. 3b), 0.5 mol% DPhBdT/DPhCzT and TCI-DPhCzT (Fig. 3c), respectively, shows nearly identical prompt and delayed spectra. More importantly, even with 0.1 mol% isomer doping, the above doping systems show effective room-temperature ultralong phosphorescence (Supplementary Fig. 6). Meanwhile, the phosphorescent emission from crystalline powders was stable in air (Supplementary Fig. 8) and their doped polymer films also showed room-temperature ultralong phosphorescence (Supplementary Fig. 9).

As for the the prompt emission (Figs. 3d-f), the fluorescence of Bd/Lab-Cz, CPhBd/CPhCz and DPhBdT/DPhCzT is red-shifted with increasing dopant content, implying that Lab-Cz could benefit the development of deep-blue emitters as compared to those based on commercial Cz[25]. Moreover, the distinct differences (solid lines in Figs. 3d-f) between the prompt emissions from each pair of isomers indicate that Cz and Bd own totally different electron-donating capabilities. In addition, the well-resolved fluorescence in Figs. 3d and f indicates that the emissions are from the local-excited (LE) states, while the broad fluorescence in Fig. 3e is the characteristic of charge-transfer (CT) emission[18,26].

Figure 3g shows the delayed LE emission of Bd/Lab-Cz, with one band at 364-543 nm and the other newly generated band at 544-836 nm after 8 ms delay upon photoexcitation at room-temperature. The delayed component of the short wavelength band varies with the dopant concentration, which agrees with the prompt emission (dashed lines in Fig. 3d), indicating that the fluorescence of Bd is involved in the delayed emission. The long wavelength band shows the highest intensity of delayed emission at 1 mol% doping. A similar phenomenon of LE delayed emission is observed for DPhBdT/DPhCzT (Fig. 3i). For CPhBd/CPhCz in Fig. 3h, the negligible CT delayed emission and obvious LE delayed emission with a maximum at 5 mol%

should be resulted from CT to LE intersystem crossing[26,27]. The delayed emission characteristics indicate that singlet and triplet excited states are simultaneously generated (Supplementary Fig. 10). Furthermore, the representative photographs of the isomer doping with varying concentrations are shown in Figs. 3j-l.

Room-temperature ultralong phosphorescence based on the isomer doping differs from most design paradigms[1,7-9,14,15,17,20,28]. The very similar molecular structure and size (Supplementary Fig. 11) allow the isomers to interact tightly[28] and generate beneficial defects to store excitation energy. To explore the mechanism, transient absorption was obtained by using the absorbance spectrum at 8 ms after photo-excitation minus that before photo-excitation[20], so that the delayed emission (negative absorption) and transient absorption (positive absorption) spectra were synchronously recorded in Figs. 4a-c and Supplementary Fig. 12. The broad absorption bands with peaks located at 460-475 nm were ascribed to radical ions[20], which were generated from charge separation. Without doping (black lines in Figs. 4a-c), spectra traced noise with photoexcitation ceased after 8 ms, indicating that charge-separated states were not generated in the Lab-Cz, Lab-CPhCz and Lab-DPhCzT crystals. Therefore, their reported ultralong phosphorescence was not observed by naked eye (Figs. 1a, 2d and 3g-i)[1,6,7]. While with doping (coloured lines in Figs. 4a-c), delayed emission and transient absorption of charge-separated states were simultaneously captured, indicating that ultralong phosphorescence was resulted from charge-separated states[20]. Further comparing 5 mol% CPhBd/CPhCz with CPhBd (Supplementary Fig. 13a), transient absorption spectra from 8 ms to 1 s show that the absorption and emission intensities are decreasing simultaneously with time, while the noise spectrum of CPhBd at 8 ms delay after photoexcitation implies no charge-separated states in the CPhBd crystals.

Owing to the different electron-donating capabilities, Cz and Bd moieties in close proximity could act as a micro planar heterojunction to generate photoinduced charge-separated states. To validate our hypothesis, we designed the 5 mol% cross doping systems of Bd/CPhCz, Bd/DPhCzT, CPhBd/Cz and DPhBdT/Cz. By comparing the prompt emission at 77 K with the delayed emission at room-temperature (Fig. 4d), the 5 mol% cross doping systems were found to emit ultralong phosphorescence with peaks located at 525-675 nm, which were from the newly generated charge-separated states (Supplementary Fig. 13b). The photographs of their ultralong phosphorescence are shown in Fig. 4e.

To further elucidate the mechanism, we studied the simple Bd/Cz doping system as an example (Fig. 4f). The highest occupied molecular orbital (HOMO) and lowest unoccupied molecular orbital (LUMO) energy levels were calculated from Supplementary Fig. 14. During photoexcitation, two types of charge transfer could occur between Bd and Cz, inducing the generation of Cz radical anions (Supplementary Fig. 15) and Bd radical cations[20]. Meanwhile, the Cz radical anions diffuse in the crystals and the Bd radical cations are trapped by defects, forming charge-separated states. Consequently, ultralong phosphorescence is resulted from gradual charge recombination of charge-separated states in the trap-detrap model of defects.

In summary, comparison between lab-synthesized and commercial sources of Cz, followed by optimization of HPLC offers a feasible solution to the impurity conundrums, which is applicable to other systems, such as commercial dibenzothiophene and dibenzofuran (Supplementary Fig. 16). Our studies reveal that the widespread isomer Bd in commercial Cz can be synchronously derived into many organic functional materials, which forms the isomer doping systems to activate ultralong phosphorescence. The identification of Bd molecular

structure opens completely different molecular design principles to manage triplet states in developing organic functional materials. This discovery also drives us to design and study the isomer effect on various organic functional materials, which is on-going in our lab.

References

1. An, Z. et al. Stabilizing triplet excited states for ultralong organic phosphorescence. *Nat. Mater.* **14**, 685-690 (2015).
2. Uoyama, H., Goushi, K., Shizu, K., Nomura, H. & Adachi, C. Highly efficient organic light-emitting diodes from delayed fluorescence. *Nature* **492**, 234-238 (2012).
3. Hamze, R. et al. Eliminating nonradiative decay in Cu(I) emitters: >99% quantum efficiency and microsecond lifetime. *Science* **363**, 601-606 (2019).
4. Ai, X. et al. Efficient radical-based light-emitting diodes with doublet emission. *Nature* **563**, 536-540 (2018).
5. Sandanayaka, A. S. D. et al. Indication of current-injection lasing from an organic semiconductor. *Appl. Phys. Express* **12**, 061010 (2019).
6. Bilen, C. S., Harrison, N. & Morantz, D. J. Unusual room temperature afterglow in some crystalline organic compounds. *Nature* **271**, 235-237 (1978).
7. Cai, S. et al. Visible-light-excited ultralong organic phosphorescence by manipulating intermolecular interactions. *Adv. Mater.* **29**, 1701244 (2017).
8. Xie, Y., Ge, Y., Peng, Q., Li, C., Li, Q. & Li, Z. How the molecular packing affects the room temperature phosphorescence in pure organic compounds: ingenious molecular design, detailed crystal analysis, and rational theoretical calculations. *Adv. Mater.* **29**, 1606829 (2017).
9. Xiong, Y. et al. Designing efficient and ultralong pure organic room-temperature phosphorescent materials by structural isomerism. *Angew. Chem. Int. Ed.* **57**, 7997-8001 (2018).
10. Zhang, T., Wang, X., An, Z., Fang, Z., Zhang, Y. & Yuan, W. Z. Pure organic persistent room-temperature phosphorescence at both crystalline and amorphous states. *ChemPhysChem* **19**, 2389-2396 (2018).
11. Gong, Y. et al. Achieving persistent room temperature phosphorescence and remarkable mechanochromism from pure organic luminogens. *Adv. Mater.* **27**, 6195-6201 (2015).
12. Yang, Z. et al. Intermolecular electronic coupling of organic units for efficient persistent room-temperature phosphorescence. *Angew. Chem. Int. Ed.* **55**, 2181-2185 (2016).
13. Fateminia, S. M. A., Mao, Z., Xu, S., Yang, Z., Chi, Z. & Liu, B. Organic nanocrystals with bright red persistent room-temperature phosphorescence for biological applications. *Angew. Chem. Int. Ed.* **56**, 12160-12164 (2017).
14. Kenry, Chen, C. & Liu, B. Enhancing the performance of pure organic room-temperature phosphorescent luminophores. *Nat. Commun.* **10**, 2111 (2019).
15. Xue, P. et al. Correction: Bright persistent luminescence from pure organic molecules through a moderate intermolecular heavy atom effect. *Chem. Sci.* **8**, 6691-6691 (2017).
16. Gu, L. et al. Dynamic ultralong organic phosphorescence by photoactivation. *Angew. Chem. Int. Ed.* **57**, 8425-8431 (2018).
17. Zhao, W. et al. Boosting the efficiency of organic persistent room-temperature phosphorescence by intramolecular triplet-triplet energy transfer. *Nat. Commun.* **10**, 1595 (2019).
18. Mao, Z. et al. Two-photon-excited ultralong organic room temperature phosphorescence by dual-channel triplet harvesting. *Chem. Sci.* **10**, 7352-7357 (2019).

19. Li, Y., Gecevicius, M. & Qiu, J. Long persistent phosphors—from fundamentals to applications. *Chem. Soc. Rev.* **45**, 2090-2136 (2016).
20. Kabe, R. & Adachi, C. Organic long persistent luminescence. *Nature* **550**, 384-387 (2017).
21. Lastusaari, M. et al. The bologna stone: history's first persistent luminescent material. *Eur. J. Mineral* **24**, 885-890 (2012).
22. Matsuzawa, T., Aoki, Y., Takeuchi, N. & Murayama, Y. A new long phosphorescent phosphor with high brightness, $SrAl_2O_4$:Eu^{2+}, Dy^{3+}. *J. Electrochem. Soc.* **143**, 2670-2673 (1996).
23. Clapp, D. B. The phosphorescence of tetraphenylmethane and certain related substances. *J. Am. Chem. Soc.* **61**, 523-524 (1939).
24. Graebe, C. & Glaser, C. *Ber. Dtsch. Chem. Ges.* **5**, 12 (1872).
25. Feng, H., Zeng, J., Yin, P. et al. Tuning molecular emission of organic emitters from fluorescence to phosphorescence through push-pull electronic effects. *Nat. Commun.* **11**, 2617 (2020).
26. Chen, C. et al. Intramolecular charge transfer controls switching between room temperature phosphorescence and thermally activated delayed fluorescence. *Angew. Chem. Int. Ed.* **57**, 16407-16411 (2018).
27. Noda, H. et al. Critical role of intermediate electronic states for spin-flip processes in charge-transfer-type organic molecules with multiple donors and acceptors. *Nat. Mater.* **18**, 1084-1090 (2019).
28. Bolton, O., Lee, K., Kim, H.-J., Lin, K. Y. & Kim, J. Activating efficient phosphorescence from purely organic materials by crystal design. *Nat. Chem.* **3**, 205-210 (2011).

Acknowledgments

This study was supported by the Singapore National Research Foundation (NRF) Competitive Research Program (R279-000-483-281), NRF Investigatorship (R279-000-444-281) and National University of Singapore (R279-000-482-133).

Author contributions

C.C. and B.L. designed the experiments. C.C. optimized HPLC and grew crystals. C.C., Z.C., Z.Y., Z.M. and Z.Y. contributed to optical characterizations. C.C. and K.C.C. synthesized all compounds. A.S.B. and C.C. solved crystal structures. C.C. and B.L. discussed the results and drafted the manuscript. B.L. supervised the project. All authors contributed to the proofreading.

Competing interests

The authors declare no competing interests.

Additional information

Supplementary information is available online.

Reprints and permissions information is available at www.nature.com/reprints.

Correspondence and requests for materials should be addressed to B.L.

Fig. 1 | Paradox of ultralong phosphorescence carbazole. a, Photographs of TCI-Cz and Lab-Cz crystals at daylight, 365 nm irradiation ON/OFF, and their single crystal structures with unit cell parameters. **b**,**c**, HPLC spectra of TCI-Cz crystals monitored at 294 and 346 nm with 95/5 to 50/50 acetonitrile (ACN)-water ratio (v/v) and chemical structures of Cz and Bd. **d**, The commercial source (e.g. TCI, J&K, SIGMA-ALDRICH, aladdin) of Cz, mixed with its isomer of Bd.

Fig. 2 | Impurity effect on carbazole derivatives. a,**b**, HPLC spectra monitored at the onset absorption of 346 nm for Cz (**a**) and 354 nm for CPhCz (**b**) from commercial and lab-synthesized sources, respectively. The elapsed time aberrations caused by injections were shifted by setting Lab-Cz and Lab-CPhCz as the reference, respectively. **c**, Chemical structures of CPhCz, CPhBd, DPhCzT and DPhBdT. **d**, Photographs of CPhCz and DPhCzT crystalline powders at daylight, 365 nm irradiation ON/OFF, and their single crystal structures with unit cell parameters. TCI-CPhCz and TCI-DPhCzT were synthesized from TCI-Cz. Lab-CPhCz and Lab-DPhCzT were synthesized from Lab-Cz.

Fig. 3 | Emission characteristics with different isomer doping concentrations. a-c, Photoluminescence (PL) spectra of crystalline powders resolved into components of prompt and delayed 8ms at room-temperature (RT) in air; 0.5 mol% Bd/Lab-Cz and TCI-Cz (**a**), 0.5 mol% CPhBd/CPhCz and TCI-CPhCz (**b**), 0.5 mol% DPhBdT/DPhCzT and TCI-DPhCzT (**c**). **d-f**, Prompt components of 0 mol%, 0.5 mol%, 1 mol%, 5 mol%, 10 mol% and 100 mol% isomer dopants; Bd/Lab-Cz (**d**), CPhBd/CPhCz (**e**) and DPhBdT/DPhCzT (**f**). **g-i**, Delayed 8 ms components of 0 mol%, 0.5 mol%, 1 mol%, 5 mol%, 10 mol% and 100 mol% isomer dopants after 365 nm excitation off; Bd/Lab-Cz (**g**), CPhBd/CPhCz (**h**) and DPhBdT/DPhCzT (**i**). **j-l**, Photographs of crystalline powders with 0.5 mol%, 1 mol%, 5 mol% and 10 mol% isomer dopants of Bd/Cz (**j**), CPhBd/CPhCz (**k**) and DPhBdT/DPhCzT (**l**). 310 nm excitation was used for the prompt spectra in **a**,**c**,**d** and 365 nm excitation for all other measurements.

Fig. 4 | Transient absorption, PL and ultralong phosphorescence mechanism. a-c, Photoinduced transient absorption (TA) of crystalline powders with 0 mol%, 1 mol%, 5 mol% and 10 mol% isomer dopants; Bd/Lab-Cz (**a**), CPhBd/CPhCz (**b**) and DPhBdT/DPhCzT (**c**). **d**, Emission of prompt at 77 K and delayed 8 ms at RT with 5 mol% cross doping systems of Bd/CPhCz, Bd/DPhCzT, CPhBd/Cz and DPhBdT/Cz crystalline powders. **e**, Photographs of crystalline powders under 365 nm ON, OFF, OFF 0.2 s and OFF 1 s. **f**, Proposed mechanism of ultralong phosphorescence (Phos.) with Bd/Cz as an example. Left, charge transfer during photoexcitation; *Type I*, electrons from the LUMO of Bd are transferred to the LUMO of Cz; *Type II*, electrons from the HOMO of Bd are transferred to the HOMO of Cz. Middle, charge-separated states are formed with Cz radical anions diffusing to the neighbour Cz, while Bd radical cations are trapped by the defects. Note that the intrinsic lattice defects may occur spontaneously during crystal growth. Right, singlets (e.g. S_1) and triplets (e.g. T_1) are generated from the charge recombination (CR) and intersystem crossing (ISC) of S_1 to T_1 is enabled.

Methods

The syntheses, isolation of Bd from TCI-Cz, preparation of doping systems and polymer films, growth of single crystals, photographs and time-dependent density functional theory (TD-DFT) calculations are fully described in Supplementary Methods (see Supplementary Information).

Materials. Commercial carbazoles were obtained from TCI (Product of Japan, C0032-100 g), J&K (Product of Beijing, 601413-250 g), Sigma-Aldrich (Product of Germany, C5132-100 g), and Aladdin (Product of Shanghai, C104875-100 g), and were further recrystallized from toluene before using. After customized synthesis from Arch Bioscience Company, Bd was further purified by column (5/95, v/v, EA/hexane) and then recrystallized from hexane. White sheet crystals were obtained (~5%, total purification yield), which have a different odor from Lab-Cz. Commercial dibenzothiophene was purchased from Sigma-Aldrich (Product of Belgium, D32202-25 g). Commercial dibenzofuran was purchased from TCI (Product of Japan, D0147-25 g). 2-Aminobiphenyl was purchased from Combi-Blocks (Product of USA, QS7870-25 g). Biphenyl-2-thiol was ordered from ChemCollect GmbH (Product of Germany, ChemCol-DP000316-5 g). Tetrahydrofuran (THF) was distilled with sodium and benzophenone. All solvents were HPLC grade from Fisher Chemical unless noted, and ultra-pure water was produced by SMART2PURE of ThermoFisher Scientific. All other chemicals were obtained from commercial sources and directly used as received unless noted.

Synthesis of Lab-Cz[29,30] (Supplementary Scheme 1). 2-Aminobiphenyl (0.85g, 5.0 mmol) was dissolved in a degassed solution containing 6.0 mL of ultra-pure water and 1.0 mL of concentrated sulfuric acid at 50 ^{o}C. After stirring at 50 ^{o}C for 5 min, the resulting solution was cooled to 0 ^{o}C in an ice-water bath, and a solution of 0.42 g (6.1 mmol) of sodium nitrite in 4.7 mL of ultra-pure water was added dropwise. The solution was stirred in the ice-water bath for 30 min. A solution of 0.56 g (8.6 mmol) of sodium azide in 3.5 mL of ultra-pure water was added dropwise into the cold solution and the mixture was further stirred for 1 h. The mixture was then filtered and washed with 100 mL of 2 M potassium carbonate solution for 3 times and then with 300 mL of ultra-pure water for 5 times. Afterward, the filtrate was dissolved with dichloromethane (DCM) and purified using column chromatography with DCM/hexane (1/3, v/v) as the eluent to yield 2-azidobiphenyl as a light-yellow oil (0.94 g, 4.8 mmol, 96% yield). The above procedures were repeated several times to produce sufficient amount of 2-azidobiphenyl.

2-Azidobiphenyl (4.0 g, 23.7 mmol) was then dissolved in 60 mL of acetone and added into a mixture containing 100 mL of acetone and 100 mL of ultra-pure water. 5.0 g of silica gel was subsequently added to the mixture and stirred for 24 h under the illumination of two HITACHI F6T5 6W fluorescent lamps, which changed the mixture from colourless to brown. The detailed setup for this photochemical step is shown in the Supplementary Fig. 17. Furthermore, the reaction solvent (260 mL) was maintained by adding acetone every 8 h. The whole reaction was covered by tinfoil. After removing the solvent by rotary evaporator, the mixture was purified using column chromatography with DCM/hexane (1/3, v/v) as the eluent. The white powder of carbazole was further purified using column chromatography two more times with ethyl acetate/hexane (5/95, v/v) and DCM/hexane (1/2, v/v) as

the eluent, respectively. After 3 times of column purification, the product was recrystallized from toluene to yield carbazole (1.2 g, 7.2 mmol, 30% yield) as white sheet crystals. The melting point of Lab-Cz was 246.9 ^{o}C and its comparison with commercial carbazole is listed in Supplementary Fig. 18.

General. HPLC purifications were conducted by using XBridege® Prep C18 OBD™ 5 μm, 50 mm × 150 mm column with 20.00 mL/min based on Waters 2545 Binary Gradient Module, Waters 2707 Autosampler and Waters Fraction Collector III. Injection volume for Cz purification was 1500 μL each at 10.0 mg/mL and injection volume for CPhCz purification was 1700 μL each at 4.0 mg/mL. DPhCzT was not sufficiently soluble in methanol or ACN and hence it could not reveal the impurity peak by HPLC based on C18 column. Purifications with silica gel column chromatography were performed using DAVISIL® silica LC60A 40-63 micro purchased from GRACE and monitored by TLC silica gel plates with 0.2-0.25 mm coating thickness from SANPONT. NMR spectra were performed with a Bruker Avance-III 400 NanoBay HD NMR spectrometer at ambient temperature. High-resolution mass spectrometry (HRMS) was investigated with a Bruker AmaZon X LC-MS for electrospray ionization. Cyclic voltammetry was performed to calculate HOMO[26] by BioLogic VMP-300 in a DCM (99.9%, Super Dry, stabilized, J&K Seal) solution containing 5×10^{-4} M sample and 0.1 M Bu_4NPF_6 electrolyte. Electrodes: working (glassy carbon), counter (Pt disk), reference (Ag/AgCl, calibrated against ferrocene), 100 $mV\cdot s^{-1}$. LUMO was determined by further measuring ultraviolet/visible absorption with Hitachi U-3900. Melting point (Mpt) was measured with differential scanning calorimetry (DSC). The instrument model was NETZSCH DSC 204 F1 Phoenix. 10 K/min was used for the heating procedure under the protection of nitrogen. Mpt was recorded with the DSC curves from the second heating process. The Mpts were the onset values, which were determined by 'NETZSCH Proteus Thermal Analysis' software. UV-visible absorption spectra of solution and solid were performed on Shimadzu UV-1700 and UV-3600 ultraviolet-visible-near-infrared (UV-Vis-NIR) spectrometers, respectively. X-ray diffraction experiments were carried out on a 4-circle goniometer Kappa geometry Bruker D8 Venture diffractometer with a PHOTON 100 CMOS active pixel sensor detector.

Optical measurements. PL spectra of 5 mol% Bd/Lab-Cz, 5 mol% CPhBd/CPhCz and 5 mol% DPhBdT/DPhCzT crystalline powders in air and vacuum were measured by Edinburgh FLS980 using OXFORD Optistat DN as the sample holder. After vacuum-pumping for 30 min, the emission of crystalline samples in vacuum was measured. Transient decay spectra, temperature-dependent photoluminescence spectra and PL quantum yield (PLQY) were carried out using a Jobin Yvon-Horiba FL-3 spectrofluorometer and equipped with a calibrated integrating sphere. Notably, PLQY of these doping systems was randomly fluctuant, which was probably caused by the emission intensity changes with prolonging the photo-irradiation[16], and hence the PLQY was not reported here. Time-resolved PL spectra (room-temperature and 77 K)[18] and photo-induced transient absorption spectra[20] were obtained at ambient temperature in air through Ocean Optics QE65 Pro CCD with Ocean Optics LED-365 and LED-310 as excitation sources and Ocean Optics DH-2000-BAL as UV-VIS-NIR light source, which were assembled according to the references.

Data availability

The data that support the findings of this study are available from C.C. and L.B. upon reasonable request. X-ray crystallographic data for structures reported here have been deposited in the Cambridge Crystallographic Data Centre (CCDC), under deposition numbers CCDC 1953802 to 1953811 and 2019581 to 2019589. These data can be obtained free of charge from the Cambridge Crystallographic Data Centre *via* www.ccdc.cam.ac.uk/data_request/cif.

References

29. Ullah, E., McNulty, J. & Robertson, A. Highly chemoselective mono-Suzuki arylation reactions on all three dichlorobenzene isomers and applications development. *Eur. J. Org. Chem.* **2012**, 2127-2131 (2012).
30. Yang, L., Zhang, Y., Zou, X., Lu, H. & Li, G. Visible-light-promoted intramolecular C-H amination in aqueous solution: synthesis of carbazole. *Green Chem.* **20**, 1362-1366 (2018).

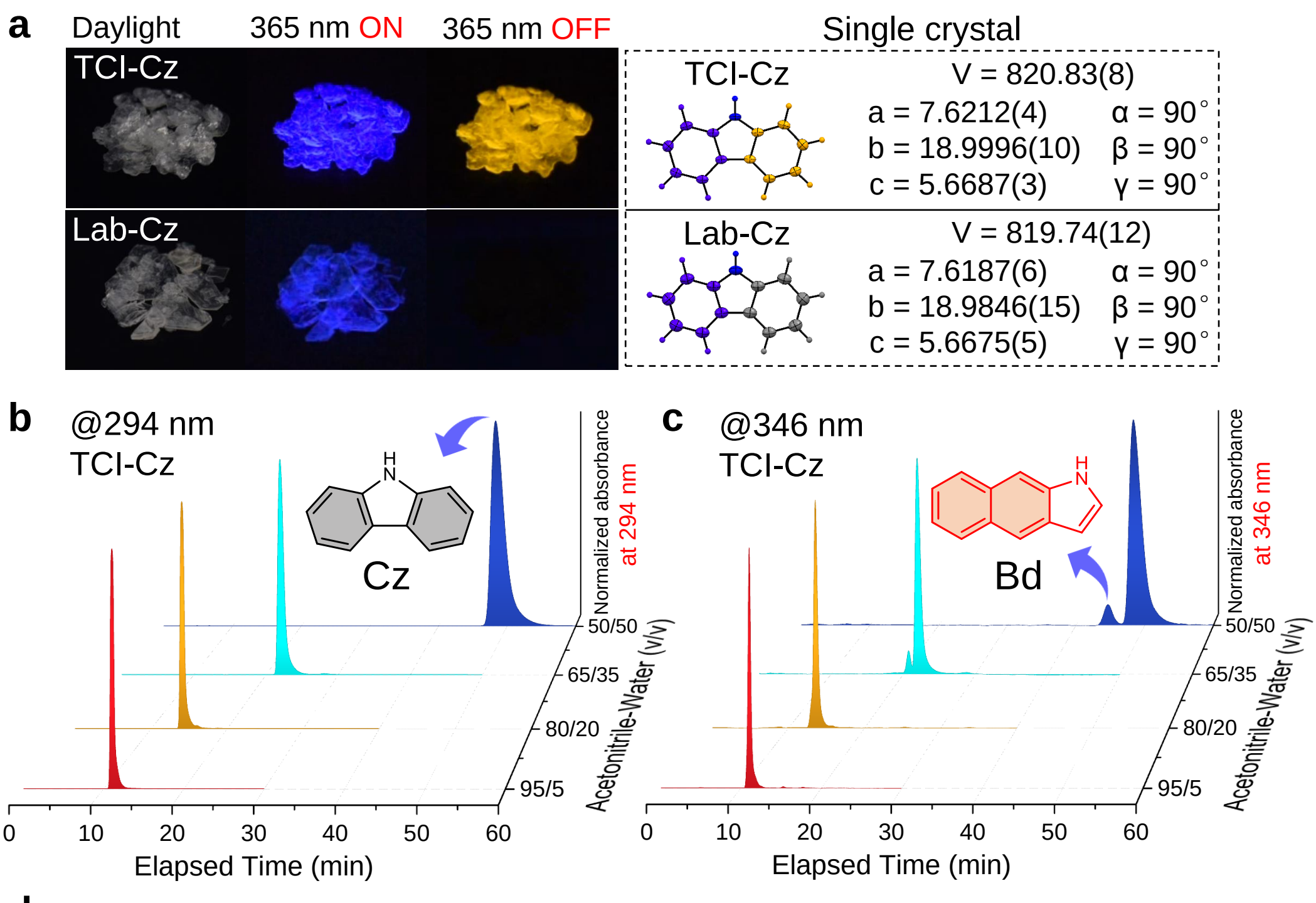
a
Daylight
365 nm ON
365 nm OFF
TCl-Cz
Lab-Cz
Single crystal
TCl-Cz
V = 820.83(8)
a = 7.6212(4) α = 90°
b = 18.9996(10) β = 90°
c = 5.6687(3) γ = 90°
Lab-Cz
V = 819.74(12)
a = 7.6187(6) α = 90°
b = 18.9846(15) β = 90°
c = 5.6675(5) γ = 90°
b
@294 nm
TCl-Cz
Cz
Normalized absorbance at 294 nm
50/50
65/35
80/20
95/5
Acetonitrile-Water (v/v)
0 10 20 30 40 50 60
Elapsed Time (min)
c
@346 nm
TCl-Cz
Bd
Normalized absorbance at 346 nm
50/50
65/35
80/20
95/5
Acetonitrile-Water (v/v)
0 10 20 30 40 50 60
Elapsed Time (min)

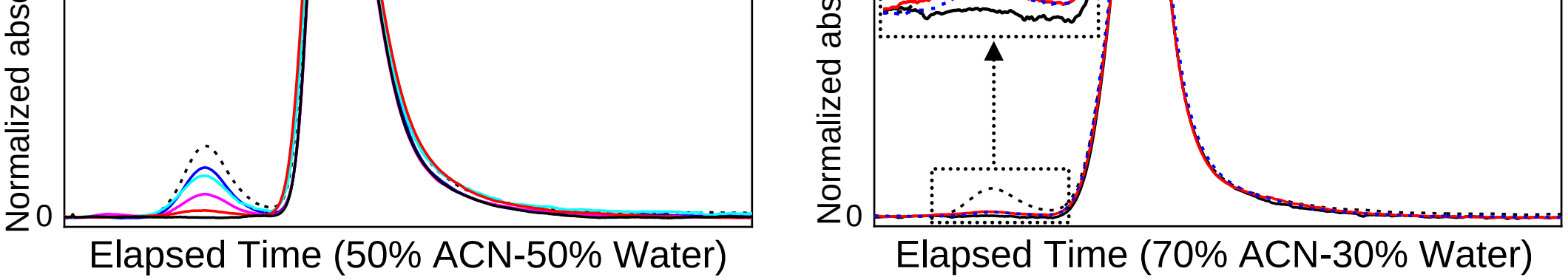
Normalized abs
0
Elapsed Time (50% ACN-50% Water)
Normalized abs
0
Elapsed Time (70% ACN-30% Water)

c

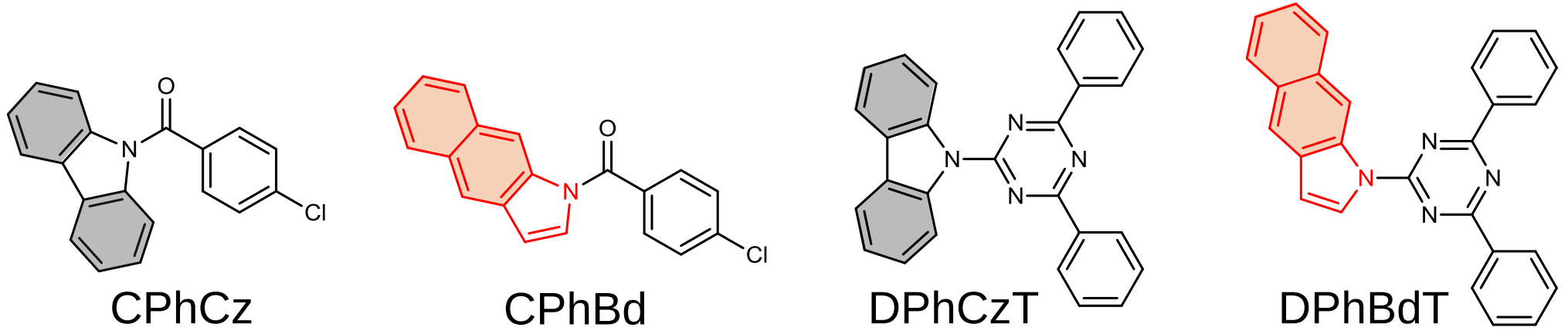
O
N
Cl
CPhCz
O
N
Cl
CPhBd
N
N
N
N
DPhCzT
N
N
N
N
DPhBdT

d

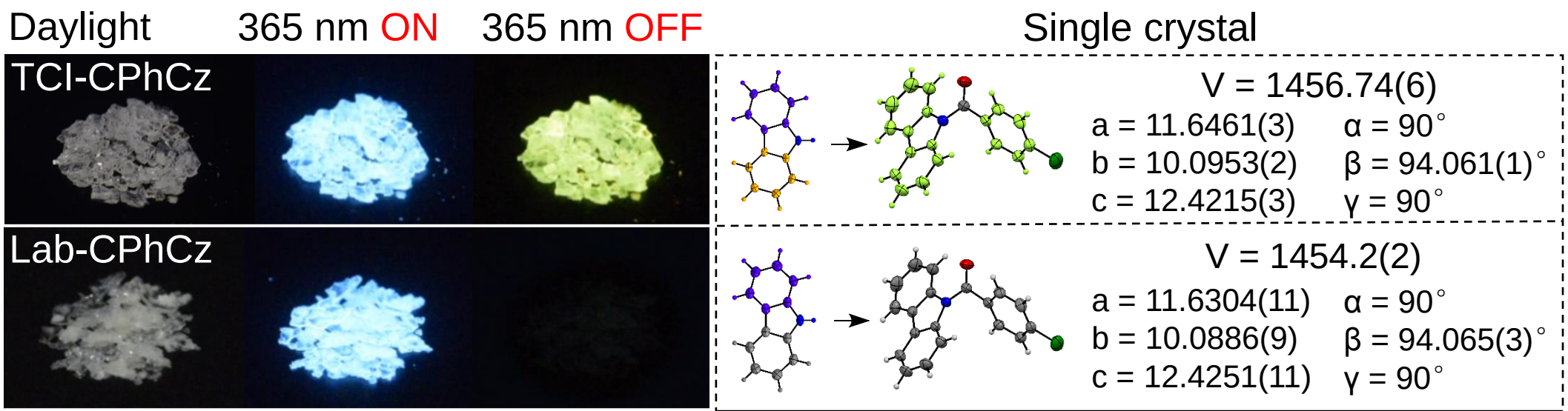
Daylight
365 nm ON
365 nm OFF
TCI-CPhCz
Lab-CPhCz
Single crystal
V = 1456.74(6)
a = 11.6461(3) α = 90°
b = 10.0953(2) β = 94.061(1)°
c = 12.4215(3) γ = 90°
V = 1454.2(2)
a = 11.6304(11) α = 90°
b = 10.0886(9) β = 94.065(3)°
c = 12.4251(11) γ = 90°

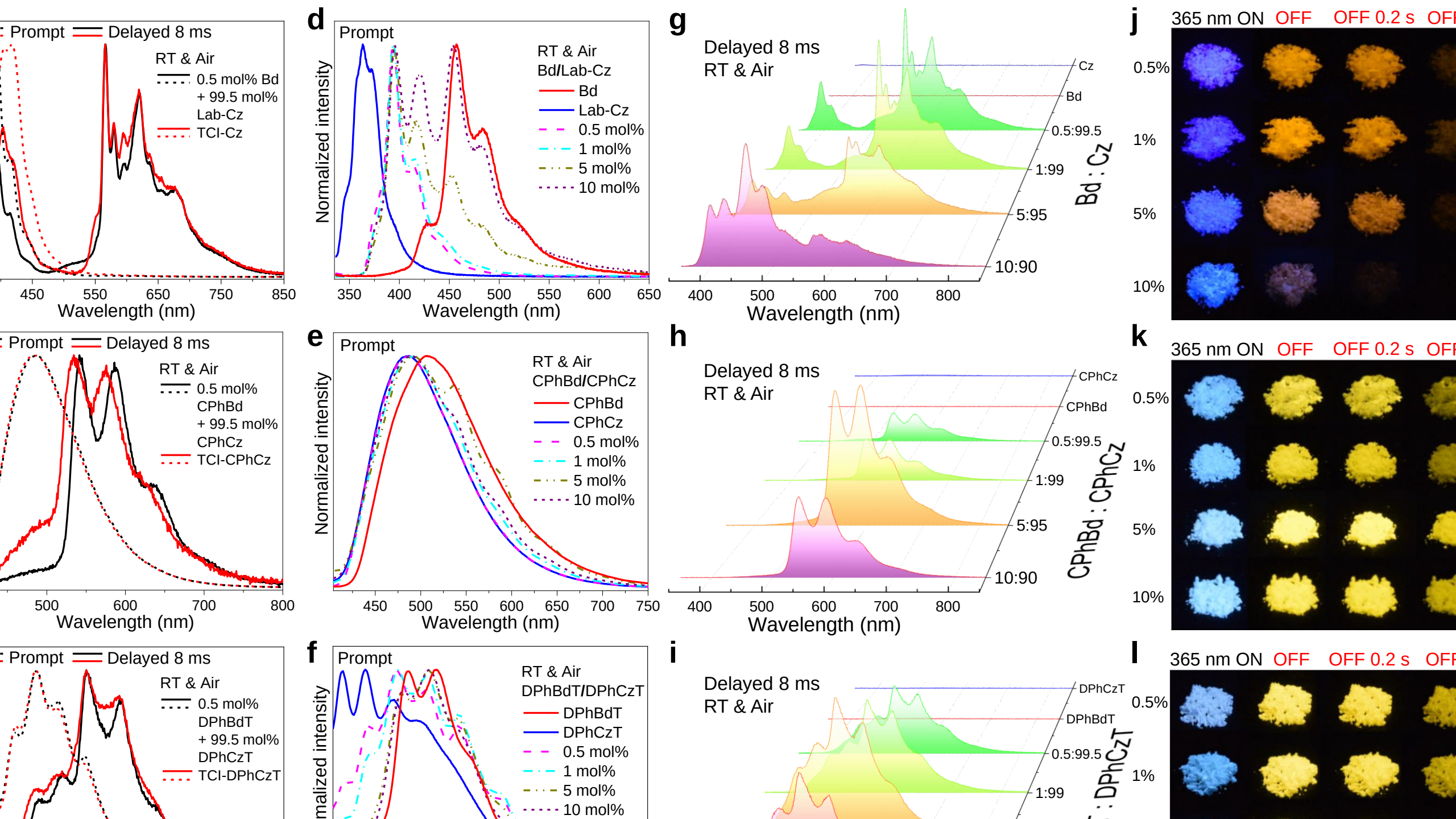
Prompt
Delayed 8 ms
RT & Air
0.5 mol% Bd
+ 99.5 mol%
Lab-Cz
TCI-Cz
Wavelength (nm)
d
Normalized intensity
RT & Air
Bd/Lab-Cz
Bd
Lab-Cz
0.5 mol%
1 mol%
5 mol%
10 mol%
g
Delayed 8 ms
RT & Air
Cz
Bd
0.5:99.5
1:99
5:95
10:90
Bd : Cz
j
365 nm ON
OFF
OFF 0.2 s
0.5%
1%
5%
10%
0.5 mol%
CPhBd
+ 99.5 mol%
CPhCz
TCI-CPhCz
e
RT & Air
CPhBd/CPhCz
CPhBd
CPhCz
h
CPhCz
CPhBd
CPhBd : CPhCz
k
0.5 mol%
DPhBdT
+ 99.5 mol%
DPhCzT
TCI-DPhCzT
f
RT & Air
DPhBdT/DPhCzT
DPhBdT
DPhCzT
i
DPhCzT
DPhBdT
l

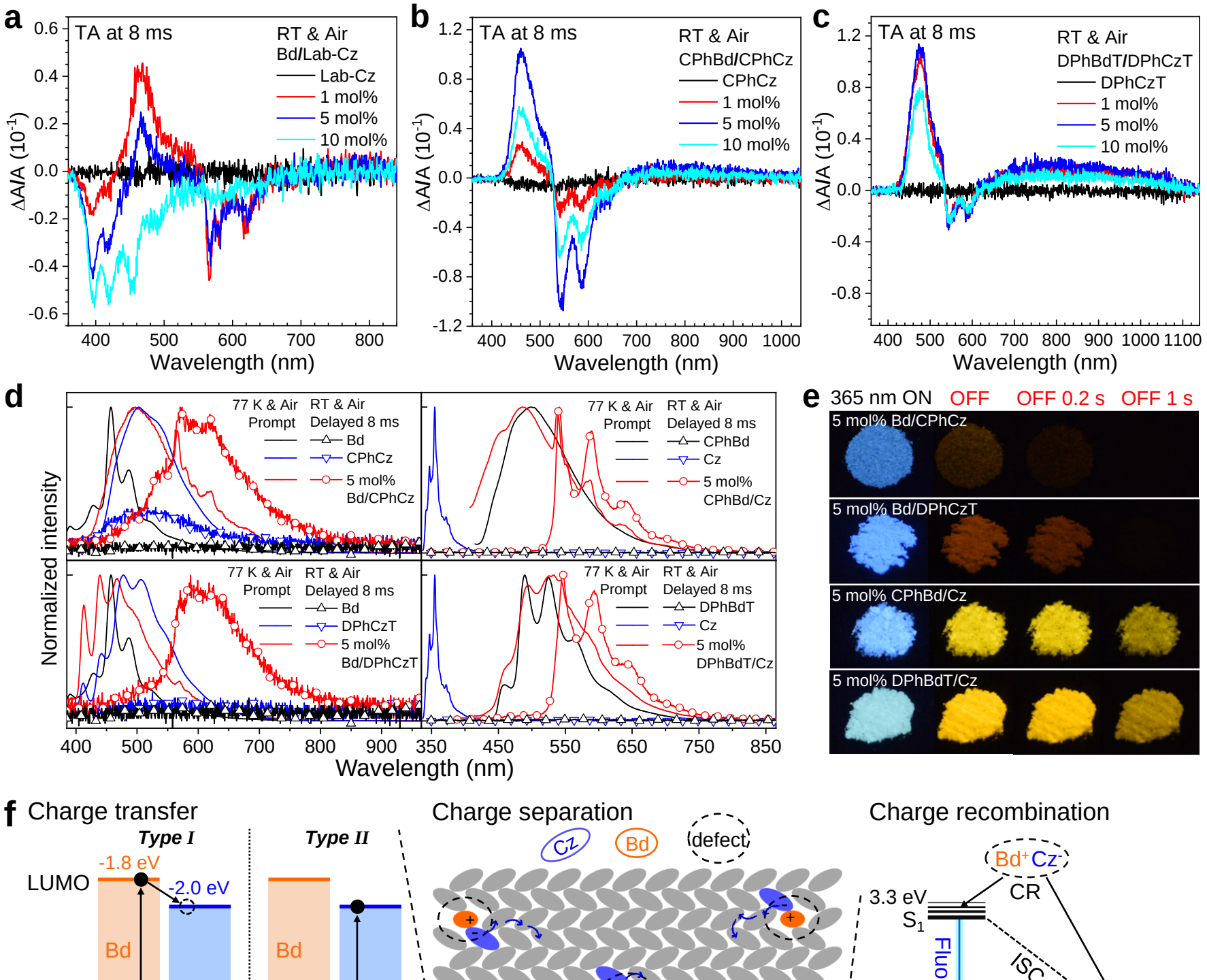
a
TA at 8 ms
RT & Air
Bd/Lab-Cz
Lab-Cz
1 mol%
5 mol%
10 mol%
ΔA/A (10⁻¹)
Wavelength (nm)
b
TA at 8 ms
RT & Air
CPhBd/CPhCz
CPhCz
1 mol%
5 mol%
10 mol%
ΔA/A (10⁻¹)
Wavelength (nm)
c
TA at 8 ms
RT & Air
DPhBdT/DPhCzT
DPhCzT
1 mol%
5 mol%
10 mol%
ΔA/A (10⁻¹)
Wavelength (nm)
d
77 K & Air Prompt
RT & Air Delayed 8 ms
Bd
CPhCz
5 mol% Bd/CPhCz
CPhBd
Cz
5 mol% CPhBd/Cz
DPhCzT
5 mol% Bd/DPhCzT
DPhBdT
5 mol% DPhBdT/Cz
Normalized intensity
Wavelength (nm)
e
365 nm ON
OFF
OFF 0.2 s
OFF 1 s
5 mol% Bd/CPhCz
5 mol% Bd/DPhCzT
5 mol% CPhBd/Cz
5 mol% DPhBdT/Cz
f
Charge transfer
Type I
Type II
LUMO
-1.8 eV
-2.0 eV
Bd
Charge separation
Cz
Bd
defect
Charge recombination
Bd⁺Cz⁻
CR
3.3 eV
S1
Fluo
ISC